Article

J. Mex. Chem. Soc. **2025**, *69*(1)
Special Issue

ISSN-e 2594-0317

MCM-41 Acid as a Sustainable Material from Waste Polystyrene

Marco Jared Niño-Castellanos[1], Eduardo Terrés-Rojas[2], Deyanira Angeles-Beltrán*[1]

[1]Universidad Autónoma Metropolitana, Departamento de Ciencias Básicas. Av. San Pablo No. 420, Azcapotzalco, Mexico City, C.P. 02128, Mexico.
[2]Instituto Mexicano del Petróleo, Eje Central Lázaro Cárdenas No. 152, Col. San Bartolo Atepehuacan, C.P. 07730, México, D.F., C.P. 07730, México

***Corresponding author:** Deyanira Angeles-Beltrán, email: dab@azc.uam.mx

Received June 1st, 2024; Accepted September 25th, 2024.

DOI: http://dx.doi.org/10.29356/jmcs.v69i1.2314

Abstract. This study incorporated expanded polystyrene (PS) from waste packaging into the mesoporous material MCM-41 to obtain PS-MCM-41. Both materials were obtained at room temperature, assisted by the ultrasound technique, and functionalized with sulfonated polystyrene (PSSA, Polystyrene Sulfonic Acid) to obtain MCM-41-PSSA and PS-MCM-41-PSSA. The evolution of the pore structures of the synthesized materials was studied using XRD. The functionalized materials' pore size, specific area, and pore volume were reduced. In addition, the thermal stability of PS-modified MCM-41 was improved concerning the parent material. The NH_3-TPD technique showed increased strong acid sites, with MCM-41-PSSA being the most acidic material. Incorporating waste material into a silicon-based mesoporous material and its functionalization with sulfonic groups allows the development of a sustainable heterogeneous material with potential applications in heterogeneous acid catalysis.
Keywords: MCM-41-PSSA; acid solid; sustainable.

Resumen. En este estudio se incorporó poliestireno expandido (PS) proveniente de empaques de desecho al material mesoporoso MCM-41 para obtener PS-MCM-41. Ambos materiales fueron obtenidos a temperatura ambiente, asistidos por la técnica de ultrasonido, y funcionalizados con poliestireno sulfonado (PSSA, Polystyrene Sulfonic Acid) para obtener MCM-41-PSSA y PS-MCM-41-PSSA. La evolución de las estructuras porosas de los materiales sintetizados se estudió mediante DRX. Se redujo el tamaño de poro, el área específica y el volumen de poro de los materiales funcionalizados. Además, la estabilidad térmica del MCM-41 modificado con PS mejoró con respecto al material original. La técnica NH_3-TPD mostró un aumento de los sitios ácidos fuertes, siendo el MCM-41-PSSA el material más ácido. La incorporación de material de desecho en un material mesoporoso basado en silicio y su funcionalización con grupos sulfónicos permite el desarrollo de un material heterogéneo sostenible con potenciales aplicaciones en catálisis ácida heterogénea.
Palabras clave: MCM-41-PSSA; sólido ácido; sostenible.

Introduction

Polystyrene (PS), with chemical formula $(C_8H_8)_n$, is a thermoplastic polymer made of styrene monomer chains. It is an amorphous material with molecular weight Mw =100,000 - 400,000 g/mol. Its main characteristics are low specific weight, transparency, gloss, absence of color, low shrinkage, and ease of manufacture. Polystyrene is one of the most widely used materials in various sectors of daily life. However,

J. Mex. Chem. Soc. **2025**, *69*(1)
Special Issue

ISSN-e 2594-0317

despite its advantages and low production costs, the useful life of this material is usually concise. In addition, massive consumption and lack of effective treatment after its use have become serious environmental problems due to the amount of waste in soil and water [1-3]. Plastics constitute the largest category of marine litter, representing at least 85 % of total waste [4]. Research indicates that most plastics collected for recycling are packaging and packing materials (62 %), of which PS represents only 5 % [5]. Additionally, several studies have detected the presence of microplastics in the digestive tract of numerous marine species, such as mollusks, cetaceans, bivalves, pinnipeds, and zooplankton, which shows that almost all commonly used polymers, especially polyethylene, and polystyrene, remain in the environment for hundreds of years, causing high pollution in the affected habitats [6]. In recent years, interest in using polystyrene has increased, especially in developing new organic-inorganic hybrid materials. For example, polystyrene has been incorporated as an additive in ceramic materials, as in the case of MCM-41, and it has been demonstrated that PS can be coated with silica-based materials to generate ceramic-polymeric hybrid materials [7]. However, research in this field is still limited.

The mesoporous material MCM-41 (Mobil Composition of Matter No. 41), synthesized by Mobil Oil Corporation in 1992, presents a porous structure in a hexagonal arrangement. Owing to its characteristics and versatility, it has been the subject of intense study and experimentation, as it has a high specific surface area, uniform pore size, excellent thermal and chemical stability, and a profusion of silanol groups (Si-OH) that allow surface chemical modification, functionalization, and easy separation from the reaction media [8]. A distinguishing feature of MCM-41 is the presence of two defined surfaces: internal (pores) and external (particles). Regioselective surface modification with functional groups makes MCM-41 versatile and allows it to perform specific tasks [9]. Surface-functionalized mesoporous materials are of great interest because of their potential applications in various areas of science, such as catalysis, adsorption, chromatography, nanotechnology, metal ion extraction, and printing for molecular recognition [10]. MCM-41 has mesopores with a high specific area (>1000 m^2/g), channels with pore diameter from 1.5 to 10 nm arranged in a hexagonal structure, and a large pore volume (>1.0 cm^3/g). These characteristics have opened new opportunities for the design of new adsorbents and heterogeneous catalysts [11]. Surface modification of MCM-41 with acidic functional groups such as -SO_3H and -COOH [12] has been used as a solid acid catalyst for chemical transformation reactions to obtain value-added products. Polystyrene Sulfonic Acid (PSSA) is an excellent functional group for catalysis because of its properties. The high concentration of uniformly distributed acid sites makes it suitable for specific organic reactions, such as hydration and esterification of olefins, alcohol dehydration, alkylation of phenols, hydration of alkenes, and hydrolysis of esters [13,14].

Many organic chemical transformations require the presence of acid catalysts, such as epoxide ring-opening reactions associated with nucleophiles. These reactions are important because they provide suitable routes for obtaining various products of interest and act as intermediates in multiple chemical reactions, as documented in numerous publications [15]. An epoxide is an ether group arranged in a ring with two carbon atoms and one oxygen atom, forming an equilateral triangular structure. With its internal tension, this structure confers higher reactivity to the compound. In addition, epoxides are versatile intermediates in organic synthesis and can react with various reagents, including electrophiles, nucleophiles, acids, bases, reducing agents, and oxidizing agents [16]. Although epoxides can be opened in acidic, basic, or neutral environments, the process proceeds more rapidly under acidic conditions [17]. However, this type of reaction often requires excess amines and extreme conditions such as elevated temperatures.

Therefore, using solid catalysts that are reusable, sustainable, and efficient can be beneficial for carrying out these organic transformations. The aim is to develop alternatives to heterogeneous catalysts that offer better reaction yields and simultaneously contribute to the synthesis of sustainable catalysts aligned with the principles of green chemistry.

For the above reasons and to reuse waste PS in a material with proven efficiency in various chemical processes, in this research, it was proposed, for the first time, to incorporate PS in the rapid ultrasound-assisted synthesis of MCM-41 to explore the properties of the mesoporous silica obtained. Secondly, we sought to acidify MCM-41 with sulfonated PS (PSSA) and, in addition, to functionalize the obtained MCM-41 with PS from the synthesis (PS-MCM-41-PSSA). Finally, the structural, thermal, chemical, and acidic properties of the mesoporous solids obtained were compared. The ultrasound technique was used, which has proven to be effective in synthesizing these materials because acoustic cavitation generates high temperatures and local pressures, favoring the adequate formation of the material. This technique also improves certain textural properties, such as the specific area. Acidifying MCM-41 by "post-synthesis" functionalization makes it

J. Mex. Chem. Soc. **2025**, *69*(1)
Special Issue

ISSN-e 2594-0317

possible to obtain acidic materials functional in chemical transformation reactions that often require homogeneous liquid catalysts. An example is the opening of epoxides, which are used to obtain amino alcohols, critical intermediates in synthesizing biologically active compounds [15].

Experimental methodology

Ultrasound-assisted synthesis of MCM-41. In a 250 mL Teflon vessel, 0.3 g of cetyltrimethylammonium bromide (CTABr, Aldrich) was dissolved in a solution of 16 g of ammonium hydroxide (NH_4OH, Aldrich 35 wt. %) and 63 g of deionized water; the mixture was kept under stirring until a homogeneous solution was obtained. Then 1.36 g tetraethyl orthosilicate 98 wt.% (TEOS, Aldrich) was added dropwise under vigorous stirring. The resulting solution was sonicated using a Bransonic model 5210E-DTH ultrasound generator with a frequency of 47 kHz and a power of 140 W at 30 °C for 2 h. The molar composition of the mixture was determined using a Bransonic model 5210E-DTH ultrasound generator with a frequency of 47 kHz and a power of 140 W at 30 °C for two hours. The molar composition of the reaction mixture was 1 TEOS: 0.125 CTABr: 69 NH_4OH: 525 H_2O.
The resulting precipitate was filtered under vacuum, washed with deionized water, dried at room temperature, and calcined at 600 °C at a heating rate of 2 °C/min for 6 h in an inert (nitrogen) atmosphere [18]. The white solid obtained was labeled MCM-41.

Synthesis of PS-MCM-41

To obtain the PS-modified material, the same procedure as describe in the previous point was followed, but before adding TEOS, 0.025 g of expanded PS (average sphere size of 4 mm) without last treatment and obtained from the protection plate of a household appliance) was added to the solution of CTABr, NH_4OH, and deionized water. Ultrasonic treatment, drying, and calcination were performed in the same way as described above. The white solid obtained was labeled PS-MCM-41.

Polystyrene Sulfonic Acid (PSSA)

First, the sulfonating agent was obtained by mixing 1 mL dichloromethane (CH_2Cl_2, Mayer) and 0.3 mL of acetic anhydride ($(CH_3CO)_2O$, Aldrich) in a flask under inert conditions using nitrogen gas. The mixture was cooled to 0°C, vigorous stirring of 0.2 mL, and 90 % v/v sulfuric acid (H_2SO_4, Aldrich) was added until a homogeneous solution was obtained. Moreover, a round flask dissolved 1 g of waste-expanded polystyrene (PS) in 10 mL of dichloromethane (CH_2Cl_2). The sulfonating agent was added for two hours at 40 °C while stirring. To stop the sulfonation, 1 mL of 2-propanol was added. The resulting residue was washed with deionized water until a color change from yellow to white was observed. Finally, the product was dried at 60 °C for 3 h [19].

Synthesis of MCM-41-PSSA

Previously synthesized MCM-41 (300 mg) was mixed in a round-bottom flask with 10 mL of ethanol and 15 mg of PSSA, corresponding to 4.76 wt.% PSSA. The mixture was then stirred at 80 °C for 24 h. The final precipitate was filtered and dried at room temperature. The obtained product was labeled MCM-41-PSSA [19].

Synthesis of PS-MCM-41-PSSA

Starting from the methodology described for the synthesis of MCM-41-PSSA, it was carried out in the same way, only that in this case, the base material for the PSSA anchor was PS-MCM-41 in the exact quantities and under the same methodology.

Characterization of the materials

X-ray diffraction patterns were obtained on a Siemens D-500 Diffractometer equipped with a graphite monochromator (Cu Kλ) = 1.54 Å, in the low-angle region (from 2θ=0.5° to 10°). Thermogravimetry tests were performed from 5-800 °C with a heating ramp of 20 °C/min in a chromatographic nitrogen atmosphere with a flow rate of 20 mL/min in a Thermo SDT Q600 instrument. Fourier Transform Infrared Spectrometry was

J. Mex. Chem. Soc. **2025**, *69*(1)
Special Issue

ISSN-e 2594-0317

performed using Alpha II Bruker FT-IR Equipment in ATR mode. Scanning Electron Microscopy was performed to determine the morphology and its respective elemental analysis by EDS in a Zeiss SUPRA 55 VP equipment. Nitrogen physisorption tests were performed using a Micromeritics ASAP 2020 sortometer. The acidity tests were performed by thermodesorption program of ammonia in a Bel Japan equipment, Belcat model; the pretreatment was carried out with 100 mg of the corresponding sample in a quartz cell and subjected to a heating ramp of 5 °C/min up to 100 °C with Helium flow of 30 cm^3/min, maintained for 90 minutes, subsequently, the cell was cooled down to 30 °C and maintained for 10 minutes. The adsorption was performed with NH_3 (%5 in He) for 10 min, and then He (30 cm^3/min) was passed again for 10 min. Finally, the sample was subjected to programmed temperature desorption (TPD) with a heating ramp of 10 °C/min up to 750 °C with a He flow of 30 cm^3/min and a stabilization time of 20 min. Solid Magnetic Resonance was performed using a Bruker Advance II300 with a rotational speed of 8 kHz. The materials' morphological characteristics and pore shapes were analyzed by high-resolution transmission electron microscopy (TEM) using a JEM-ARM200CF instrument (JEOL, Tokyo, Japan). The solid powders were supported on a Cu grid, maintaining a good dispersion of the particles, and the samples were analyzed at an accelerating voltage of 200 KV.

Catalytic evaluation of acidic materials

The nucleophilic opening reaction of two epoxides with two amines under classical and microwave-assisted heating conditions was used to test and compare the acidity of PSSA-functionalized materials. Aldrich brand reagent was used without prior purification. 1.1 mmol of benzylamine or aniline 1 mmol and 1,2-Epoxy-3-phenoxypropane or cyclohexene oxide (Fig. 1) were reacted in a vial fitted with a screw cap and a small magnetic stirrer, without solvent and with 50 mg of the catalyst (MCM-41 or MCM-41-PSSA). The reaction mixture was heated to 60 °C for two hours or irradiated with microwaves (CEM Discover Labmate) at 60 °C and 50 W for 30 min. At the end of the reaction, the solid was recovered by filtration, and the remaining or crude reaction liquid was analyzed by gas FID chromatography with a coupled mass detector (Agilent 6890 Serie II Plus/Detector 5973).

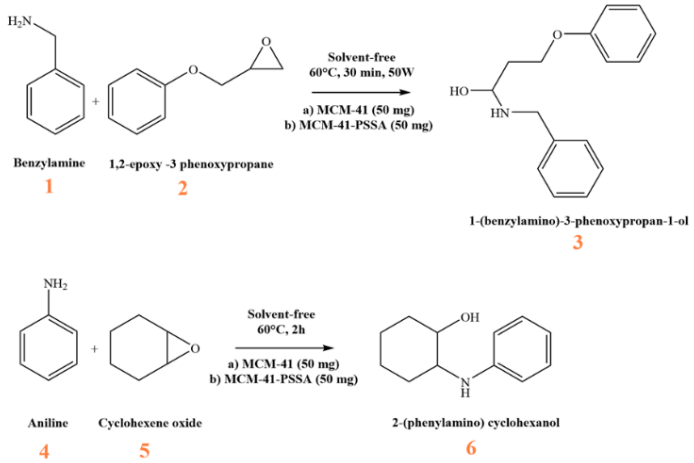

Fig. 1. Reaction schemes of the catalytic evaluation of MCM-41 and MCM-41-PSSA.

Results

X-ray diffraction

According to the comparative of X-ray diffraction patterns in Fig. 2, the presence of the characteristic peak of MCM-41, located between 2.7 and 3.1° 2θ and associated with the reflection of the (100) plane of a hexagonal structure, can be observed [20,21]. By adding PS to the synthesis of MCM-41, the peak intensity

J. Mex. Chem. Soc. **2025**, *69*(1)
Special Issue

ISSN-e 2594-0317

presented by PS-MCM-41 decreased slightly and shifted to the left; however, the MCM-41 structure was maintained. Notably, the intensity of the diffraction peak of MCM-41-PSSA abruptly reduced concerning MCM-41 because of the incorporation of PSSA inside its pores, which decreased the short-range ordering identified in the diffraction pattern [22]. With the functionalization of PS-MCM-41 with the PSSA group, the intensity of the diffraction peak (ordering) was almost completely lost; however, the porosity was not lost, and the specific area was preserved, as observed in the BET and SEM results. A summary of the interplanar distances with the respective angles of 2θ is shown in Table 1.

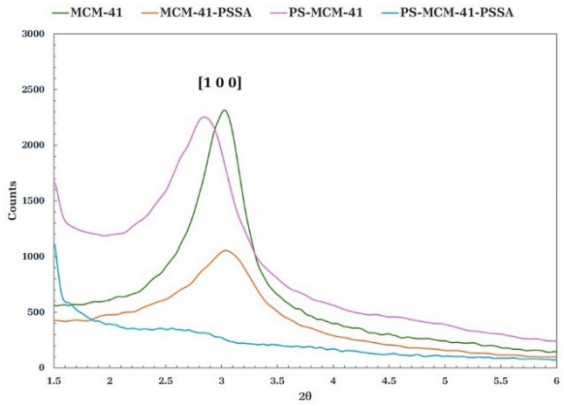

Fig. 2. Diffractograms of MCM-41, MCM-41-PSSA, PS-MCM-41 and PS-MCM-41-PSSA.

Table 1. Characteristics of materials obtained by XRD.

Sample	2θ Position of (100)	$d_{(100)}$ spacing (Å)
MCM-41	3.04	29.057
PS-MCM-41	2.95	29.860
MCM-41-PSSA	3.05	28.880
PS-MCM-41-PSSA	2.50	35.222

Fourier-transform infrared spectroscopy (FT-IR)

The spectra in Fig. 3 compares the materials obtained. For MCM-41, the characteristic bands located at 1055 cm^{-1} and 807 cm^{-1}, which are associated with Si-O-Si and Si-O stretching vibrations, respectively, can be observed. The band observed at 963 cm^{-1} is assigned to Si-OH stretching, while the absorption band at 1632 cm^{-1} corresponds to the deformation vibrations of adsorbed water molecules (δ_{H-O-H}). The presence of the broad band at 3100-3600 cm^{-1} is attributed to O-H stretching at the surface due to silanol groups with hydrogen bonds and remaining adsorbed water molecules [23]. In the FT-IR spectrum of the sample modified with Polystyrene Sulfonic Acid (PSSA), the absorption bands at 1601 cm^{-1} and 1493 cm^{-1}, characteristic of C=C stresses are appreciated, in the range from 3082 to 2921 cm^{-1} are associated with C-H stresses, while at 1030 cm^{-1}, the stretching stress corresponding to the S=O bond at 1171 cm^{-1} is related to sulfonic group stress (SO_3) [24]. The band at 755 cm^{-1} is associated with the C-S bond strain, the S-O bond vibration appears at 696 cm^{-1}, and the broadband at 3405 cm^{-1} is due to the O-H bond [25]. The FT-IR spectrum of the functionalized MCM-41-PSSA (Fig. 3) shows the characteristic bands of both compounds; the intense band at 1067 cm^{-1} is associated with Si-O-Si stretching vibrations, characteristic of the mesoporous material, whereas the bands of PSSA are located at 2981 cm^{-1}, corresponding to C-H vibrations, the band at 1643 cm^{-1} is associated with C=C vibrations

J. Mex. Chem. Soc. **2025**, *69*(1)
Special Issue

ISSN-e 2594-0317

of the aromatic ring, and the band at 963 cm^{-1} is attributed to S-O stretching [19,26]. Both MCM-41 and PS-MCM-41 were calcined before FT-IR tests, and it can be said that there was no significant difference between the infrared spectra of both materials; the PSSA-functionalized samples were not calcined.

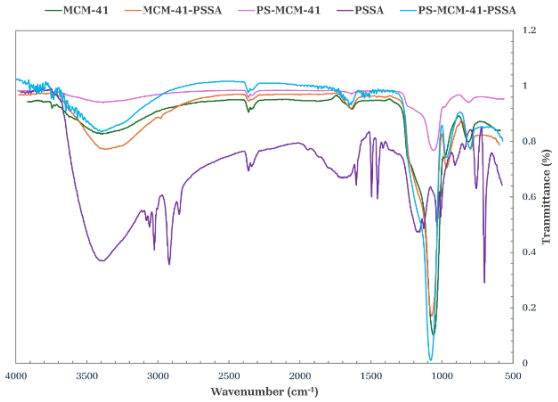

Fig. 3. FT-IR spectrums of MCM-41, MCM-41-PSSA, PS-MCM-41, PSSA and PS-MCM-41-PSSA.

Thermogravimetric analysis (TGA)

According to the thermogram shown in Fig. 4, in the weight loss curves of uncalcined MCM-41, five maxima in the weight loss rate (peak 1-5) are appreciated: peak 1 centered at 61.77 °C is associated with physically adsorbed water constituting 2.5 % of the weight loss; peak two at 152.21 °C is related to the decomposition of the compound that forms the template director of the structure, cetyltrimethylammonium bromide (CTABr) up to this point, there is a 15.27 % weight loss; peaks 3 and 4 at 184.35 °C and 281 °C, respectively, are attributed to the combustion of remaining carbon species, such as residual carbon or deposited carbon, having a cumulative weight loss of 59.46 %; and finally, peak 5, located at 350.03 °C corresponds to the dehydroxylation of the silanol groups, having a total weight loss of 64.97 % [27]. In the PSSA thermogram (Fig. 4), at 55.72 °C, a mass loss of 3.04 % was observed due to evaporation of the water in the sample. The second transition region was observed at 393.95 °C due to the degradation of the sulfonic group ($-SO_3$), also called desulfonation; the loss at this temperature is 54.42 %, and the peak of the third transition is present at 567.74 °C is the result of the side chain cleavage of the PSSA polymer, with a total weight loss of 90.47 % [28]. The thermogram obtained from the functionalized material MCM-41-PSSA (Fig. 4) shows its mass loss peaks: the first one at 69.09 °C is associated with the evaporation of water molecules present due to the interactions with the sulfonic groups, representing a loss of 10.95 % by weight; the second peak located at 239.14 °C is due to the loss of the $-HSO_3-$ groups, reaching 24.22 % loss by weight; the third peak located at 299.31 °C is due to the decomposition of the polymeric chain, reaching 24.95 % loss by weight; finally, the fourth peak at 454.97 °C is associated with the dehydroxylation of the silanol (Si-OH) groups and the decomposition of the PSSA side chain, resulting in a loss of 26.29 % by weight of the total sample [24,27,29]. The thermogram of the material with incorporated polystyrene PS-MCM-41 (Fig. 4) showed an improvement in thermal properties compared to the source material MCM-41; three losses were identified: one at 46.42°C associated with 1.29% water remaining in the material, a second loss at 262.91 °C related to the decomposition of the structuring agent (CTABr), and a third loss at 380.49 °C corresponding to the dehydroxylation of the silanol groups, associated with 38.56 % by weight of the total mass. In the case of the PS-MCM-41-PSSA material (Fig. 4), a significant mass loss was appreciated at 69.54 °C associated with the evaporation of adsorbed water, representing 25.51 % of the total mass, a second loss located at 173.44 °C, corresponding to 42.93 %. It was associated with the degradation of the anchored PSSA. TGA tests for MCM-41 and PS-MCM-41 were performed on uncalcined materials.

J. Mex. Chem. Soc. **2025**, *69*(1)
Special Issue

ISSN-e 2594-0317

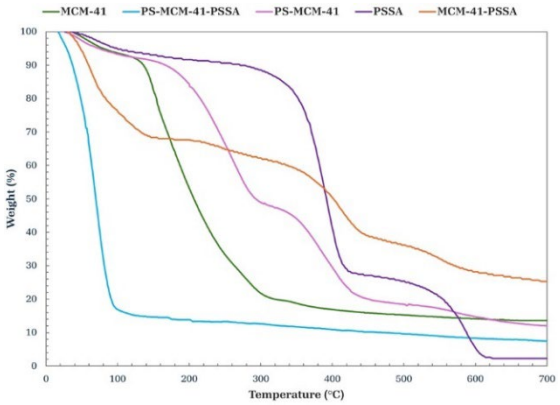

Fig. 4. Termograms of MCM-41, PS-MCM-41-PSSA, PS-MCM-41, PSSA and MCM-41-PSSA.

Nitrogen physisorption

According to the International Union of Pure and Applied Chemistry (IUPAC) classification of adsorption-desorption isotherms, the isotherms of the materials synthesized in this study (Figures 5-8) are of type IV [30]. In all the isotherms, a relatively narrow hysteresis loop, characteristic of MCM-41 materials, can be observed; therefore, it can be stated that the uniformity of the pores is maintained both at the entrance and exit and, in general, throughout the length of the pore, even with the incorporation of PS and functionalization with PSSA. Table 2 shows the textural properties of the obtained materials; taking MCM-41 as a reference, it can be said that the incorporation of PS increases the pore size and volume, which agrees with the leftward shift observed in its main peak in the X-ray diffraction pattern (Fig. 2). The MCM-41-PSSA and PS-MCM-41-PSSA materials showed decreased specific surface area, pore size, and pore volume values compared to MCM-41; however, they retained their mesoporous characteristics. The changes observed in their diffraction patterns (Fig. 2) and the loss of intensity of the principal peak are due to the incorporation of PS and PSSA inside the pores, which caused changes in the interaction of X-rays with the porous structure of these materials. Partially filled pores behave like an amorphous solid material, which consequently results in fewer pores interacting with the X-ray beam, leading to a loss of intensity of the central diffraction peak. On the other hand, although PS-MCM-41 also showed a decrease in specific surface area compared to MCM-41, the pore size and pore volume increased by 20 % and 94.12 %, respectively, due to the incorporation of PS in the synthesis, which could be beneficial for its application in adsorption processes as the capacity to accommodate bulky species in its cavities would be favored.

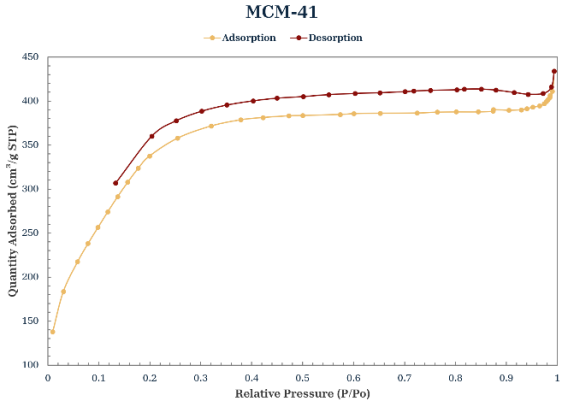

Fig. 5. Nitrogen physisorption isotherm of MCM-41.

J. Mex. Chem. Soc. **2025**, *69*(1)
Special Issue

ISSN-e 2594-0317

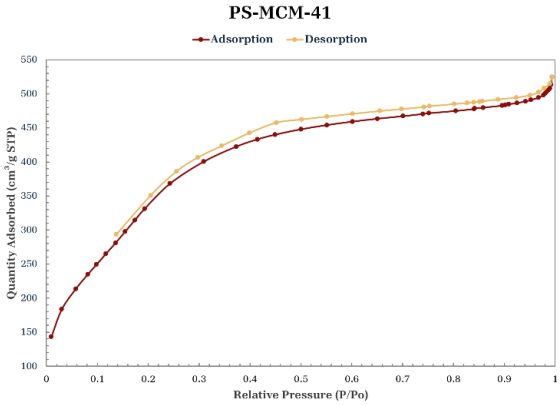

Fig. 6. Nitrogen physisorption isotherm of PS-MCM-41.

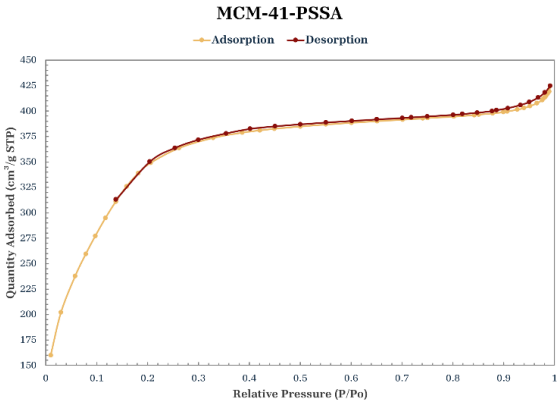

Fig. 7. Nitrogen physisorption isotherm of MCM-41-PSSA.

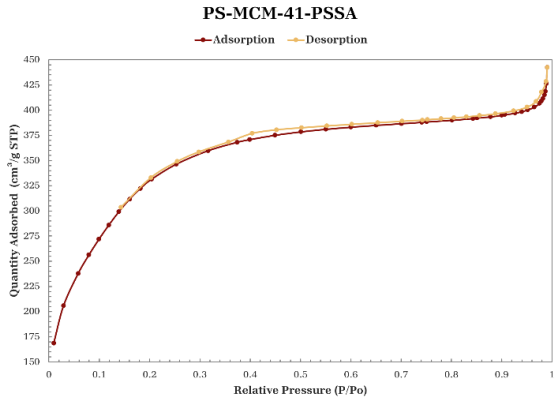

Fig. 8. Nitrogen physisorption isotherm of PS-MCM-41-PSSA.

J. Mex. Chem. Soc. **2025**, *69*(1)
Special Issue

ISSN-e 2594-0317

Table 2. Textural properties of obtained materials.

Sample	BET Surface (m^2/g)	Pore size (Å)	Pore volume (cm^3/g)
MCM-41	1329.90	20	0.51
PS-MCM-41	1314.67	24	0.99
MCM-41-PSSA	1321.02	19	0.40
PS-MCM-41-PSSA	1229.15	21	0.44

Nuclear magnetic resonance of solids (Solid-State NMR)

The spectra (Fig. 9 and 10) were obtained using the high-power decoupled direct-polarization (HPDEC) technique. The spectrum of ^{29}Si for MCM-41 (Fig. 9) showed three signals that are associated with [$Q_n = Si(OSi)_n(OH)_{4-n}$ by convention] Q^2 corresponding to geminal groups, Q^3 to free and neighboring single silanols, and Q^4 type signals corresponding to siloxane groups. Two intense signals were observed in the spectrum at δ = -102.836 and -111.329 ppm assigned to species types Q^3 and Q^4, respectively. In addition, a lower intensity signal at δ = -93.6146 ppm, associated with Q^2 species, corresponds to the MCM-41 materials described in the literature [31]. The spectrum ^{29}Si-RMN of the porous material functionalized with PSSA (Fig. 10) shows signals at δ = -103.407 and -111.899 ppm, which are attributed to the silicon groups in the silica matrix with chemical environments of Q^4 [$Si(SiO_4)$] and Q^3 [$Si(SiO_3)OH$], respectively. This was not observed in the parent MCM-41, which was attributed to the modification of the material with the added PSSA and modifying the Q^4 environment of the silicon atom bonding [32].

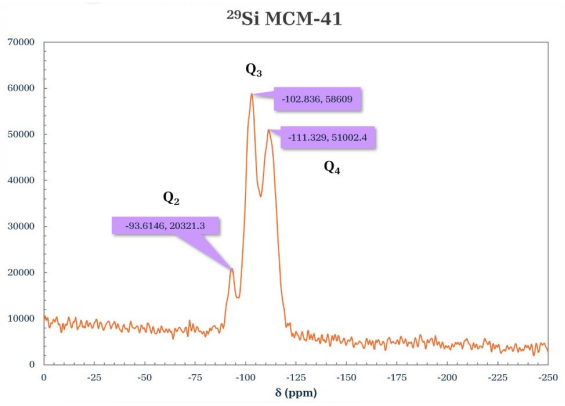

Fig. 9. ^{29}Si-RMN spectrum of MCM-41.

J. Mex. Chem. Soc. **2025**, *69*(1)
Special Issue

ISSN-e 2594-0317

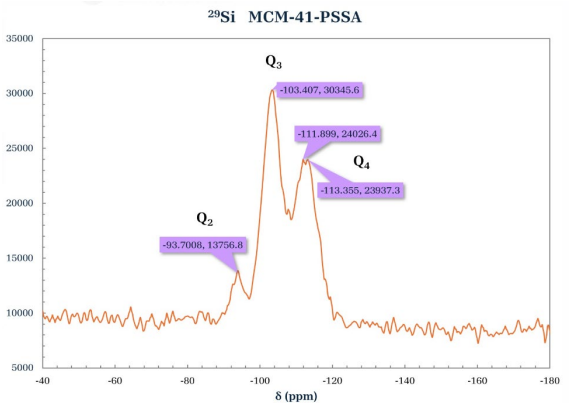

Fig. 10. ^{29}Si-RMN spectrum of MCM-41-PSSA.

Temperature-programmed desorption of ammonia (NH_3-TPD)

To study the distribution of acid sites on the surface of MCM-41, MCM-41-PSSA, and PS-MCM-41-PSSA, NH_3-TPD analysis was performed, from which ammonia desorption profiles were obtained (Fig. 11). As can be seen, it is evident that by incorporating PSSA on MCM-41 (MCM-41-PSSA), the amount of solid acid sites increases; this is due to the presence of sulfonic groups ($-SO_3H$) that give acidity to the porous material. In contrast, the PS-MCM-41-PSSA material presented a decrease in its weak, medium, and strong acid sites compared to MCM-41. For the classification of acid sites, weak acid sites were defined as those located at temperatures below 300 °C, while intermediate acid sites were identified as those found between 300 °C and 500 °C, and strong acid sites as those situated at temperatures above 500 °C [33]. Table 3 lists the total acidity of each material.

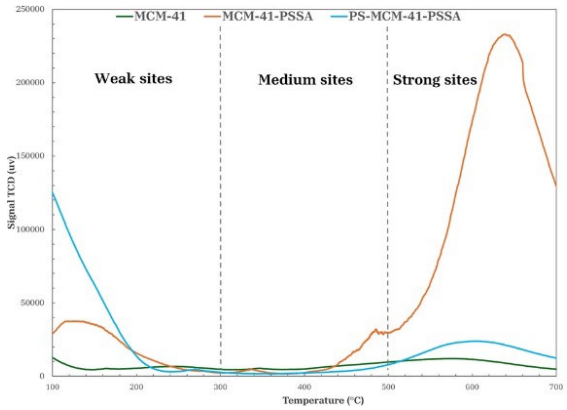

Fig. 11. NH_3-TPD profiles of MCM-41 (green), MCM-41-PSSA (orange) y PS-MCM-41-PSSA (blue).

Table 3. Total acidity values of obtained materials.

Sample	Total acidity (mmol/g)
MCM-41	3.54
MCM-41-PSSA	85.05

J. Mex. Chem. Soc. **2025**, *69*(1)
Special Issue

ISSN-e 2594-0317

X-ray spectroscopy Scanning electron microscopy (SEM) and energy-dispersive X-ray spectroscopy (EDS)

The micrographs in Figures 12-19 show the morphologies of the obtained materials. For the mesoporous MCM-41 shown in Fig. 12 and 13, it can be observed that the material consists of agglomerates of amorphous particles with mostly smooth surfaces, and these particles exhibit varied sizes. It should be noted that this morphology is related to the synthesis method used since the ultrasound-assisted technique results in the formation of agglomerates with curved surfaces. Figures 14-16 show micrographs of the MCM-41 material with incorporated waste polystyrene. A mixture of different morphologies, textures, and sizes can be observed, which can be attributed to the fact that integrating polystyrene in the synthesis alters the initial morphology (Fig. 12 and 13), which comprises regular-shaped rolls or spheres. In addition, the ultrasound-assisted technique generated agglomerates of quasi-spherical particles that were also present in the final morphology. The calcination process for obtaining the mesoporous material can lead to the formation of laminar spherical structures, such as those shown in Fig. 15 for the PS-MCM-41 material. Fig. 20 shows the histograms of the particle sizes of the obtained materials, indicating the smallest particle size corresponds to MCM-41 and that the addition of PS increased the particle size. With the functionalization of both MCM-41 and PS-MCM-41 with PSSA, an increase in the particle size was also observed. The particle size classifications obtained in this study were MCM-41<PS-MCM-41<PS-MCM-41-PSSA<MCM-41-PSSA. In Fig. 21, the elemental composition of the materials is qualitatively appreciated, and Table 4 shows the elemental quantification of the materials obtained and analyzed by X-ray energy dispersive spectroscopy.

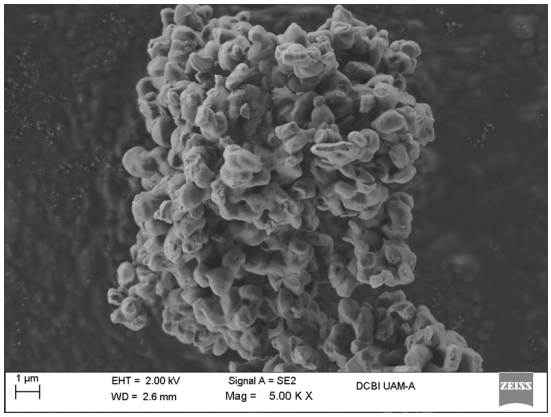

Fig. 12. SEM image of MCM-41.

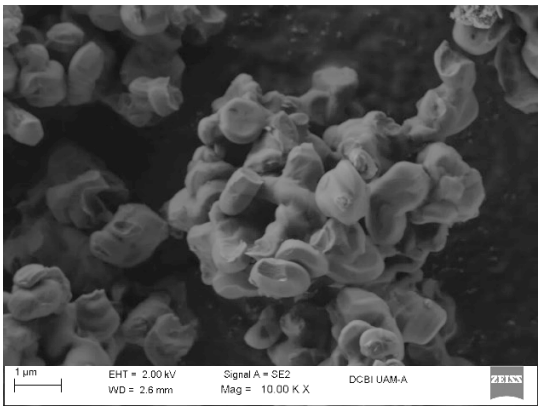

Fig. 13. SEM image of MCM-41.

J. Mex. Chem. Soc. **2025**, *69*(1)
Special Issue

ISSN-e 2594-0317

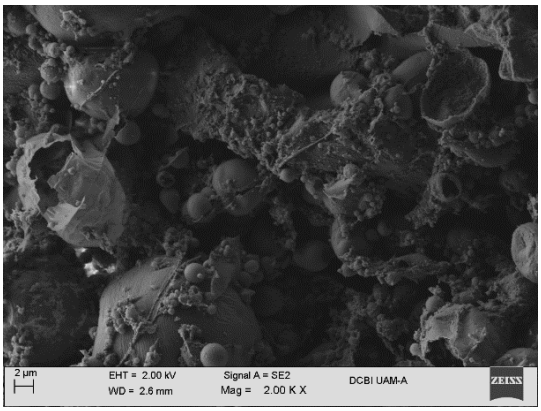

Fig. 14. SEM image of PS-MCM-41.

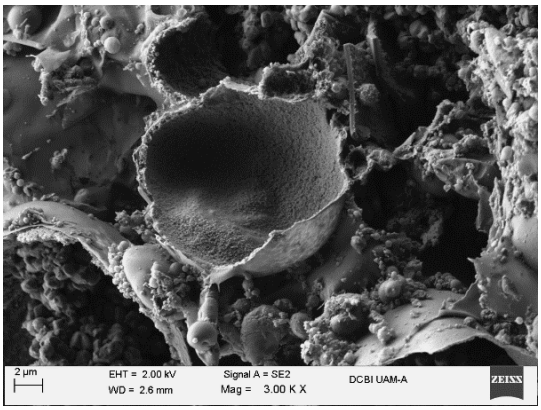

Fig. 15. SEM image of PS-MCM-41.

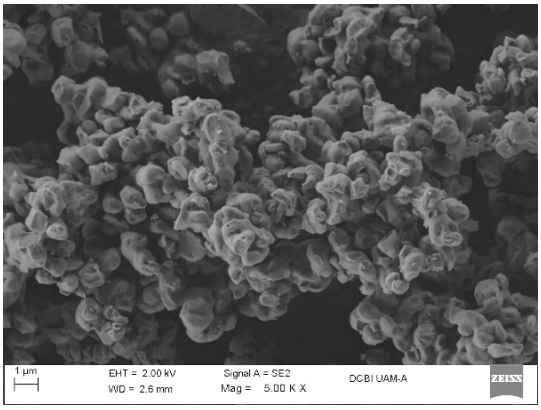

Fig. 16.SEM image of PS-MCM-41.

J. Mex. Chem. Soc. **2025**, *69*(1)
Special Issue

ISSN-e 2594-0317

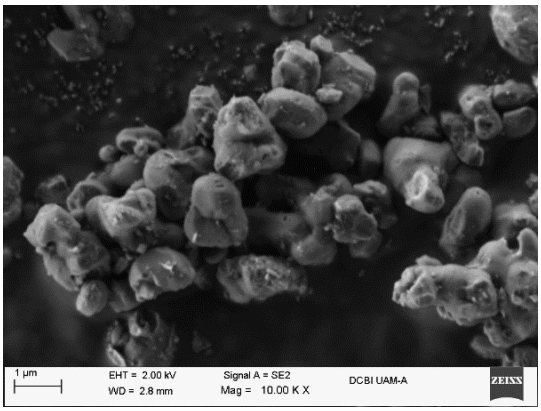

Fig. 17. SEM image of PS-MCM-41-PSSA.

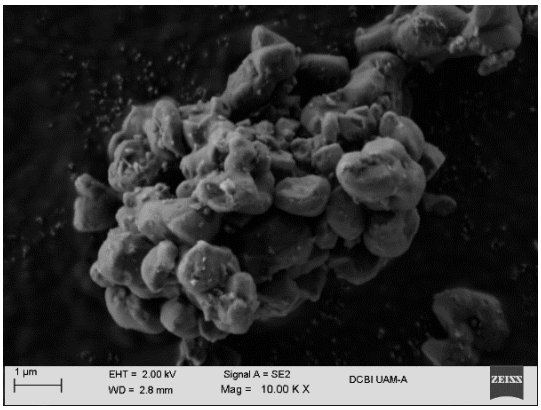

Fig. 18. SEM image of MCM-41-PSSA.

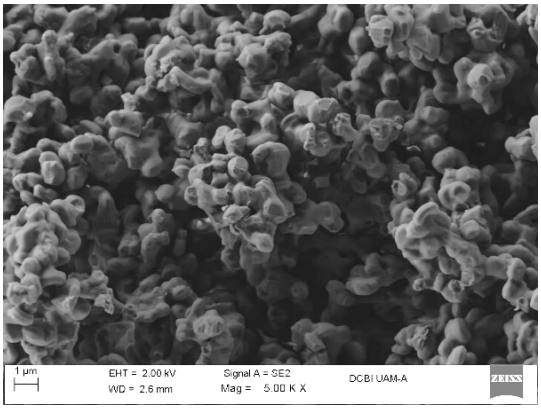

Fig. 19. SEM image of MCM-41-PSSA.

J. Mex. Chem. Soc. **2025**, *69*(1)
Special Issue

ISSN-e 2594-0317

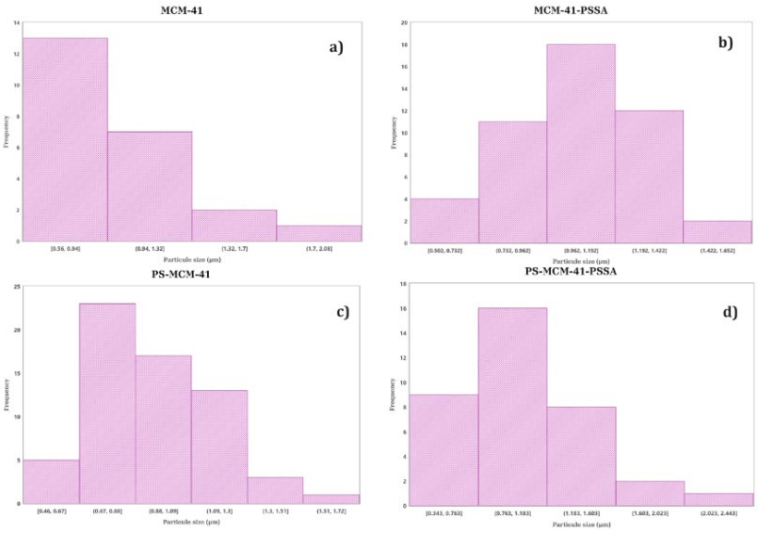

Fig. 20. Particle size histograms of **(a)** MCM-41, **(b)** MCM-41-PSSA, **(c)** PS-MCM-41 y **(d)** PS-MCM-41-PSSA.

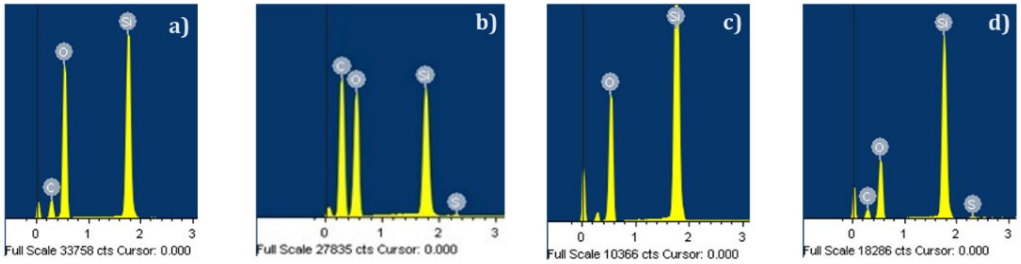

Fig. 21. EDS analysis spectrums of **(a)** MCM-41, **(b)** MCM-41-PSSA, **(c)** PS-MCM-41 y **(d)** PS-MCM-41-PSSA.

Table 4. Chemical composition obtained by EDS.

	% wt			
Element	MCM-41	MCM-41-PSSA	PS-MCM-41	PS-MCM-41-PSSA
C	18.03	19.75	-	19.99
O	55.35	48.30	48.46	40.10
Si	26.61	31.39	51.54	39.60
S	-	0.55	-	0.31

Transmission Electron Microscopy

Fig. 22 and 23 correspond to TEM micrographs of the materials the MCM-41 and MCM-41-PSSA, respectively; a more ordered arrangement can be observed for the case of the parent silicon material (MCM-41,

J. Mex. Chem. Soc. **2025**, *69*(1)
Special Issue

ISSN-e 2594-0317

Fig. 22) concerning the functionalized material (MCM-41-PSSA, Fig. 23) since the presence of the PSSA groups in the mesoporous solid altered the characteristic ordering that MCM-41 presents, which agrees with what was obtained by X-ray diffraction (Fig. 2).

The catalytic evaluation of MCM-41 (starting material) and MCM-41-PSSA (acid-functionalized) obtained the results in Table 5. The obtained product was identified by gas chromatography using an FID and masses detectors. It was verified that MCM-41-PSSA was more active than MCM-41 in obtaining reaction products under microwave-assisted and classical conditions, producing a significant increase in the yield of the reactions.

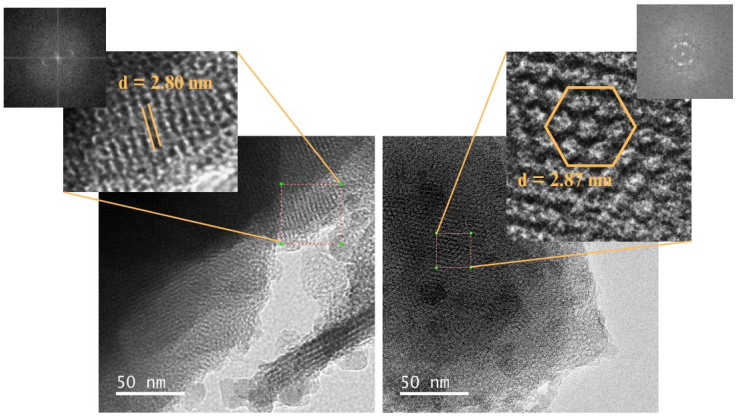

Fig. 22. TEM images of MCM-41.

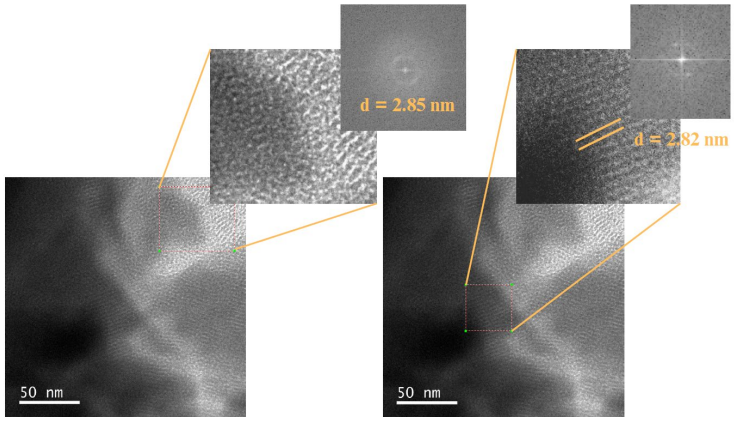

Fig. 23. TEM images of MCM-41-PSSA.

Table 5. Catalytic evaluation tests results.

Product	**% Yield**		**Evaluation reaction conditions**
	MCM-41	MCM-41-PSSA	
3	17	76	60 °C, 30 min, solvent free, MW 50 W
6	traces	61	60 °C, 2 h, solvent free

J. Mex. Chem. Soc. **2025**, *69*(1)
Special Issue

ISSN-e 2594-0317

Conclusions

To implement sustainable synthesis methodologies and processes, a mesoporous silicate modified by incorporating a waste polymer (PS-MCM-41) was synthesized and characterized using a fast ultrasound-assisted technique, which increased the pores' volume and size. However, a slight decrease in the specific area was observed, maintaining the ordering and hexagonal structure present in MCM-41. In addition, PS-MCM41 improved its thermal stability compared to MCM-41 and presented a narrower hysteresis, which improved the uniformity and definition of its pores, thus allowing thermal stresses to dissipate more efficiently. When PS-MCM-41 and MCM-41 were functionalized with PSSA, their pore sizes and volumes decreased. PSSA functionalization of MCM-41 resulted in a material with solid acid sites without a significant decrease in pore area or pore size.

Incorporating a waste polymer in MCM-41-type structures would reduce the presence of pollutants in the environment. With the sulfonation reaction of polystyrene to obtain MCM-41-PSSA, a more environmentally friendly process is obtained since the main advantage is reflected in the reduction of hazardous reagents. In this sense, research development and the application of materials that present a sustainable alternative are of interest to green chemistry since the materials developed are competitive candidates for use in heterogeneous acid catalysis.

Acknowledgements

We thank Marco Antonio Vera Ramírez (UAM-I) for the Solid-State NMR characterization of the samples and the Divisional Laboratory of Scanning Electron Microscopy of the UAM-A. To Dr. Mirella Gutiérrez Arzaluz (UAM-A) for the TPD characterization and Dr. Lifang Chen (IPN) for her support for the TEM characterization. DAB and ETR thank CONAHCyT for the SNII distinction. MJNC thanks CONAHCyT for the postgraduate fellowship awarded.

References

1. Baena-González, J.; Santamaria-Echart, A.; Aguirre, J.L.; González, S. *Waste Manage (Oxford)*. **2020**, *118*, 139-149 DOI: http://dx.doi.org/10.1016/J.WASMAN.2020.08.035.
2. Chae, Y.; An, Y. J. Sep. 01, 2018, Elsevier Ltd. DOI: http://dx.doi.org/10.1016/j.envpol.2018.05.008.
3. Compa, M.; Alomar C.; Wilcox, C.; Van Sebille, E.; Lebreton, L.; Hardesty, B. D.; Deudero, S. *Sci Total Environ.* **2019**, *678*, 188–196 DOI: http://dx.doi.org/10.1016/j.scitotenv.2019.04.355.
4. Brouwer, R.; Huang, Y.; Huizenga, T.; Frantzi, S.; Le, T.; Sandler, J.; Dijkstra, H.; Van Beukering, P.; Costa, E.; Garaventa, F.; Piazza, V. *Ocean Coast. Manag.* **2023**, *238*, 106555 DOI: http://dx.doi.org/10.1016/j.ocecoaman.2023.106555.
5. Di, J.; Reck, B. K.; Miatto, A.; Graedel, T. E. *Resour. Conserv. Recycl.* **2021**, *167*. DOI: http://dx.doi.org/10.1016/j.resconrec.2021.105440.
6. Godoy, V.; Blázquez, G.; Calero, M.; Quesada, L.; Martín-Lara, M. A. *Environ. Pollut.* **2019**, *255*. DOI: http://dx.doi.org/10.1016/j.envpol.2019.113363.
7. Chen, M.; Zhou, S.; Wu, L.; Xie, S.; Chen, Y. *Macromol. Chem. Phys.* **2005**, *206*, 1896–1902. DOI: http://dx.doi.org/10.1002/macp.200500200.
8. Lin Hu, Y.; Rong, Q.; Chen, C.; Bing Liu, X., J. *Saudi Chem. Soc.* **2023**, *27*, 101588. DOI: http://dx.doi.org/10.1016/J.JSCS.2022.101588.
9. Martínez-Edo, G.; Balmori, A.; Pontón, I.; Del Rio, A. M.; Sánchez-García, D. *MDPI*. **2018**. DOI: http://dx.doi.org/10.3390/catal8120617.
10. Alothman, Z. A. **2012**. DOI: http://dx.doi.org/10.3390/ma5122874.

J. Mex. Chem. Soc. **2025**, *69*(1)
Special Issue

ISSN-e 2594-0317

11. Jabbari, A.; Mahdavi, H.; Nikoorazm, M.; Ghorbani-Choghamarani, A. *Res. Chem. Intermed*. **2015**, *41*, 5649–5663. DOI: http://dx.doi.org/10.1007/s11164-014-1690-x.
12. Chaudhary, G.; Gupta, N.; Singh, A. P. Polyhedron. **2021**, *207*, 115348. DOI: http://dx.doi.org/10.1016/J.POLY.2021.115348.
13. Siril, P. F.; Cross, H. E.; Brown, D.R. *J. Mol. Catal A. Chem.* **2008**, *279*, 63–68. DOI: http://dx.doi.org/10.1016/j.molcata.2007.10.001.
14. Siril, P. F.; Brown, D. R. *J. Mol. Catal. A Chem.* **2006**, *252*, 125–131. DOI: http://dx.doi.org/10.1016/j.molcata.2006.02.050.
15. Thirumalaikumar, M. *Taylor and Francis Ltd*. **2022**. DOI: http://dx.doi.org/10.1080/00304948.2021.1979357.
16. Ferreira, C. E. S.; Santos-Vieira, I.; Gomes, C. R.; Balula, S. S.; Cunha-Silva, L. *Polymers (Basel)*. **2024**, *16*. DOI: http://dx.doi.org/10.3390/polym16070968.
17. Mandal, T.; Panu, K. *J. Synth. Chem.* **2024**, 13–23. DOI: http://dx.doi.org/10.22034/JSC.2024.451160.1070.
18. Vetrivel, S.; Chen, C. T.; Kao, H. M. *New J. Chem.* **2010**, *34*, 2109–2112. DOI: http://dx.doi.org/10.1039/c0nj00379d.
19. Salim, E.; Afrizal; Zilfadli, **2021**, *6*, 153–161. DOI: http://dx.doi.org/10.12962/j25493736.v6i2.1091.
20. Mokrzycki, J.; Fedyna, M.; Duraczyńska, D.; Marzec, M.; Panek, R.; Franus, W.; Bajda, T.; Karcz, R. *Materials, Jan*. **2024**, *17*, 653 DOI: http://dx.doi.org/10.3390/ma17030653.
21. www.elsevier.nl/locate/micromeso, accessed in May 2024.
22. Cuesta Zapata, P. M.; Miranda, J. F.; Orellana, F.; Gonzo, E.; Bonini, N. A. *Mater. Chem. Phys.* **2022**, *287*. DOI: http://dx.doi.org/10.1016/j.matchemphys.2022.126232.
23. Du, P. H.; Hieu, N. T.; To, T. C.; Bach, L. G.; Tinh, M. X.; Mau, T. X.; Quang, K. D. *Adv. Mater. Sci. Eng.* **2019**, *2019*. DOI: http://dx.doi.org/10.1155/2019/8573451.
24. Tian, Y.; Zhu, X.; Zhou, S.; Zhao, W.; Xu, Q.; Liu, X. *J. Bioresour. Bioprod.* **2023**, *8*, 198–213. DOI: http://dx.doi.org/10.1016/j.jobab.2023.01.003.
25. Niluroutu, N.; Shukla, A.; Dhavale, V. M.; Unni, S. M.; Bhat, S. D. *Int. J. Hydrogen Energy.* **2021**, *46*, 20640–20649. DOI: http://dx.doi.org/10.1016/j.ijhydene.2021.03.156.
26. Sakunpongpitiporn, P.; Phasuksom, K.; Paradee, N.; Sirivat, A. *RSC Adv.* **2019**, *9*, 6363–6378. DOI: http://dx.doi.org/10.1039/c8ra08801b.
27. https://pubs.acs.org/sharingguidelines, accessed in May 2024.
28. Yang, C. C.; Chiu, S. J.; Kuo, S. C. *Curr. Appl. Phys., Jan.* **2011**. DOI: http://dx.doi.org/10.1016/j.cap.2010.11.043.
29. Tran, A. T. K.; Pham, T. T.; Nguyen, Q. H.; Hoang, N. T. T.; Bui, D. T.; Nguyen, M. T.; Nguyen, M. K.; Van Der Bruggen, B. *J. Environ. Chem. Eng.* **2020**, *8*. DOI: http://dx.doi.org/10.1016/j.jece.2020.104302.
30. Thommes, M.; Kaneko, K.; Neimark, A. V.; Oliver, J. P.; Rodriguez-Reinoso, F.; Rouquerol, J.; Sing, K. S. W. *Pure Appl. Chem.* **2015**, *87*, 1051–1069. DOI: http://dx.doi.org/10.1515/pac-2014-1117.
31. Nunes, C. D.; Valente, A. A.; Pillinger, M.; Fernandes, A. C.; Romão, C. C.; Rocha, J.; Gonçalves, I. S. *J. Mater. Chem.* **2002**, *12*, 1735–1742. DOI: http://dx.doi.org/10.1039/b109678h.
32. Adam, F.; Kueh, C. W. *J. Taiwan Inst. Chem. Eng.* **2014**, *45*, 713–723. DOI: http://dx.doi.org/10.1016/j.jtice.2013.07.008.
33. Olivares, Y.; Herrera, C.; Seguel, J.; Sepúlveda, C.; Parra, C.; Pecchi, G. *Catalysts.* **2023**, *13*. DOI: http://dx.doi.org/10.3390/catal13061024.